Hindawi Publishing Corporation
International Journal of Antennas and Propagation
Volume 2015, Article ID 176202, 11 pages
http://dx.doi.org/10.1155/2015/176202

Research Article

Limited Feedback for 3D Massive MIMO under 3D-UMa and 3D-UMi Scenarios

Zheng Hu,[1] Shaoli Kang,[1,2] and Xin Su[2]

[1]*School of Electronic and Information Engineering, Beihang University, Beijing 100191, China*
[2]*State Key Laboratory of Wireless Mobile Communications, China Academy of Telecommunications Technology (CATT), Beijing 100191, China*

Correspondence should be addressed to Zheng Hu; huzheng2008168@sina.com

Received 20 December 2014; Revised 9 June 2015; Accepted 11 June 2015

Academic Editor: Stefano Selleri

For three-dimensional (3D) massive MIMO utilizing the uniform rectangular array (URA) in the base station (BS), we propose a limited feedback transmission scheme in which the channel state information (CSI) feedback operations for horizontal domain and vertical domain are separate. Compared to the traditional feedback scheme, the scheme can reduce the feedback overhead, code word index search complexity, and storage requirement. Also, based on the zenith of departure angle (ZoD) distribution in 3D-Urban Macro Cell (3D-UMa) and 3D-Urban Micro Cell (3D-UMi) scenarios, we propose the angle quantization codebook for vertical domain, while the codebook of long term evolution-advanced (LTE-Advanced) is still adopted in horizontal domain to preserve compatibility with the LTE-Advanced. Based on the angle quantization codebook, the subsampled 3-bit DFT codebook is designed for vertical domain. The system-level simulation results reveal that, to compromise the feedback overhead and system performance, 2-bit codebook for 3D-UMa scenario and 3-bit codebook for 3D-UMi scenario can meet requirements in vertical domain. The feedback period for vertical domain can also be extended appropriately to reduce the feedback overhead.

1. Introduction

Multiple-input multiple-output (MIMO) is a maturing and important technology in the 3rd Generation Partnership Project (3GPP) LTE and LTE-Advanced. Its advantages have been exploited in the past years. Recently, relying on a large excess of antennas in the BS over the terminals, massive MIMO as a promising and fascinating technology to improve energy efficiency and spectrum efficiency of future networks becomes a hot spot in academia and industry [1, 2].

Restricted to the physical space, the URA draws a lot of attention in massive MIMO system. With the use of active antenna systems (AAS), such two-dimensional (2D) antenna array can offer more spatial degrees of freedom (DoFs) in both elevation and azimuth domains in contrast to the uniform linear array (ULA). Equipped with the 2D antenna array, the BS can form beams in both elevation and azimuth domains adaptively [3]. Recently, there is a new study item for 3D MIMO which has been approved for the sake of investigation on the benefit of 2D antenna array [4].

In the traditional 2D MIMO system, the users can be just served simultaneously in different horizontal directions. However users located in the same azimuth angle cannot be served at the same time because all beams in vertical domain have the same downtilt [5]. With a 2D active antenna array, 3D MIMO can exploit the elevation dimension as well as the azimuth dimension in MIMO system. It is possible to achieve system performance improvement to meet the increasing capacity demand [6, 7].

Traditional channel models such as 2D spatial channel models (SCMs) just concentrate on the 2D propagation in the horizontal plane. Accordingly, to evaluate the performance of 3D MIMO transmission technique, the 3D channel model considering both the azimuth domain and elevation domain of signal propagation must be proposed [8, 9]. The 3GPP has

developed the 3D channel model under 3D-UMa and 3D-UMi scenarios [10].

To explore the potentials of massive MIMO, downlink transmit precoding is essential. The acquisition of CSI is crucial for the efficient precoding. The time division duplexing (TDD) system can obtain CSI based on channel reciprocity via uplink pilot training [1]. There are also many existing cellular networks based on frequency division duplexing (FDD) which obtains the CSI via uplink feedback from the user. However, the feedback overhead grows inevitably as the number of antennas increases and the code word search requires more computational complexity [11, 12]. The limited feedback is challenging for massive MIMO.

Several works have been engaged in this issue. In [11], based on the spatial correlation and channel conditions in massive MIMO systems, the authors suggest two compression methods for channel feedback to reduce the feedback overhead. In [12], a novel noncoherent trellis-coded quantization for massive MIMO is proposed. Its complexity increases linearly with the number of transmit antennas. When supporting a variable number of antennas, it could adjust flexibly the feedback overhead and does not have to change the structure of the quantizer. Literature [13] designs a noniterative two-stage precoding method with limited feedback for the interference channel in massive MIMO. The second stage precoders can compress the CSI of interfering links. Based on the compressed CSI, the task of the first stage precoders is to zero-force the interference. A hybrid limited feedback design is proposed for massive MIMO in [14]. It considers both the quantized feedback and codebook based feedback. Literature [15] proposes a codebook design for port modulation in massive MIMO system. It can offer low average bit error probability without instantaneous CSI at the transmitter, only with low feedback burden. In [16], based on the Kronecker-type approximation of the array correlation structure, the authors propose a codebook for URA deployment and the codebook is suitable for closely spaced antennas of massive MIMO. Literature [17] proposes a limited feedback transmission for 3D MIMO. It utilizes two CSI-RS ports to calculate the horizontal CSI and vertical beam gain. In [18], the authors propose a 3D MIMO beamforming scheme. Using the horizontal and vertical PMIs from the user, the scheme can improve the overall system performance relatively to the 2D MIMO system.

In this paper, for the massive MIMO equipped with the URA, we propose the scheme in which the user feeds back the CSI for horizontal domain and vertical domain separately based on the characteristics of 3D MIMO. This can reduce the code word size and search complexity. According to the characteristics of the 3D-UMa and 3D-UMi scenarios, we design the codebook for the vertical domain and reduce the feedback overhead as much as possible. Also, we propose that the feedback period for vertical domain can be extended, thus leading to the reduction of feedback overhead.

2. System Model

2.1. 3D Antenna Radiation Pattern. Here we incorporate 3D antenna radiation pattern proposed by 3GPP for the antenna elements of the BS array [10].

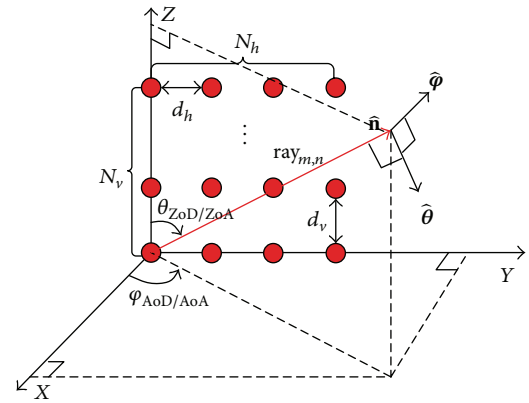

Figure 1: The coordinate system of 3D MIMO and the antenna configuration in the BS.

The horizontal radiation pattern is listed below:

$$A_{E,H}(\varphi) = -\min\left[12\left(\frac{\varphi}{\varphi_{3\,\text{dB}}}\right)^2, A_m\right], \quad \varphi_{3\,\text{dB}} = 65^\circ,\ A_m = 30\,\text{dB}. \tag{1}$$

And the vertical radiation pattern is

$$A_{E,V}(\theta) = -\min\left[12\left(\frac{\theta - 90}{\theta_{3\,\text{dB}}}\right)^2, \text{SLA}_v\right], \quad \theta_{3\,\text{dB}} = 65^\circ,\ \text{SLA}_v = 30\,\text{dB}, \tag{2}$$

where φ is the azimuth angle between the user and the boresight of the array in horizontal domain. θ is the elevation angle between the user and the boresight of the array in vertical domain. A_m is the front-to-back attenuation and SLA_v denotes sidelobe attenuation. $\varphi_{3\,\text{dB}}$ and $\theta_{3\,\text{dB}}$ are the half-power beamwidth (HPBW) in horizontal and vertical domains, respectively.

The 3D antenna pattern is

$$A_E(\theta, \varphi) = -\min\left\{-\left[A_{E,V}(\theta) + A_{E,H}(\varphi)\right], A_m\right\}. \tag{3}$$

2.2. 3D Channel Model. To evaluate the massive MIMO, here we introduce the 3D channel model of 3GPP [10]. The 3D channel model considers not only the radio propagation in the horizontal dimension but also the radio propagation in the vertical dimension in contrast to the 2D channel model.

The generation of the 3D channel includes the scenario selection, the determination of user parameters, and the channel coefficients. The channel coefficients consist of the large scale parameters and the small scale parameters. Due to space limitations, for the large scale parameters such as shadow fading and path loss refer to [10]. The generation of the small scale channel coefficients comes from a contribution of several clusters. Also each cluster contains several rays. In Figure 1, we depict a ray labeled as $\text{ray}_{m,n}$ in the coordinate system for 3D MIMO. $\text{ray}_{m,n}$ denotes the mth ray in the nth cluster. In this figure, $\hat{\mathbf{n}}$ is the direction of $\text{ray}_{m,n}$. $\hat{\boldsymbol{\theta}}$ and $\hat{\boldsymbol{\varphi}}$

are the spherical basis vectors. In the coordinate system, the zenith angle of departure (arrival) $\theta_{\mathrm{ZoD/ZoA}}$ and the azimuth angle of departure (arrival) $\varphi_{\mathrm{AoD/AoA}}$ are defined. $\theta_{\mathrm{ZoD}} = 0^{\circ}$ points to the zenith direction and $\theta_{\mathrm{ZoD/ZoA}} = 90^{\circ}$ points to the horizontal direction.

For the nth cluster which is composed of M rays, the channel coefficient of the receive-transmit element pair (u, s) is modeled as the following.

In the non-line-of-sight (NLOS) case,

$$\begin{aligned} H_{u,s,n}(t) = {} & \sqrt{\frac{P_n}{M}} \sum_{m=1}^{M} \begin{bmatrix} F_{\mathrm{rx},u,\theta}\left(\theta_{n,m,\mathrm{ZOA}}, \varphi_{n,m,\mathrm{AOA}}\right) \\ F_{\mathrm{rx},u,\varphi}\left(\theta_{n,m,\mathrm{ZOA}}, \varphi_{n,m,\mathrm{AOA}}\right) \end{bmatrix}^{T} \\ & \cdot \begin{bmatrix} \exp\left(j\Phi_{n,m}^{\theta\theta}\right) & \sqrt{\kappa_{n,m}^{-1}} \exp\left(j\Phi_{n,m}^{\theta\varphi}\right) \\ \sqrt{\kappa_{n,m}^{-1}} \exp\left(j\Phi_{n,m}^{\varphi\theta}\right) & \exp\left(j\Phi_{n,m}^{\varphi\varphi}\right) \end{bmatrix} \begin{bmatrix} F_{\mathrm{tx},s,\theta}\left(\theta_{n,m,\mathrm{ZOD}}, \varphi_{n,m,\mathrm{AOD}}\right) \\ F_{\mathrm{tx},s,\varphi}\left(\theta_{n,m,\mathrm{ZOD}}, \varphi_{n,m,\mathrm{AOD}}\right) \end{bmatrix} \exp\left(j2\pi\lambda_0^{-1}\left(\hat{\mathbf{r}}_{\mathrm{rx},n,m}^{T} \cdot \overline{\mathbf{d}}_{\mathrm{rx},u}\right)\right) \\ & \cdot \exp\left(j2\pi\lambda_0^{-1}\left(\hat{\mathbf{r}}_{\mathrm{tx},n,m}^{T} \cdot \overline{\mathbf{d}}_{\mathrm{tx},s}\right)\right) \exp\left(j2\pi\nu_{n,m}t\right). \end{aligned} \tag{4}$$

In the line-of-sight (LOS) case, let $H'_{u,s,n} = H_{u,s,n}$. The channel coefficients include a line-of-sight ray and the other channel coefficients generated by (4),

$$\begin{aligned} H_{u,s,n}(t) = {} & \sqrt{\frac{1}{K_R+1}} H'_{u,s,n}(t) + \delta(n-1) \\ & \cdot \sqrt{\frac{K_R}{K_R+1}} \begin{bmatrix} F_{\mathrm{rx},u,\theta}\left(\theta_{\mathrm{LOS,ZOA}}, \varphi_{\mathrm{LOS,AOA}}\right) \\ F_{\mathrm{rx},u,\varphi}\left(\theta_{\mathrm{LOS,ZOA}}, \varphi_{\mathrm{LOS,AOA}}\right) \end{bmatrix}^{T} \\ & \cdot \begin{bmatrix} \exp\left(j\Phi_{\mathrm{LOS}}\right) & 0 \\ 0 & -\exp\left(j\Phi_{\mathrm{LOS}}\right) \end{bmatrix} \begin{bmatrix} F_{\mathrm{tx},s,\theta}\left(\theta_{\mathrm{LOS,ZOD}}, \varphi_{\mathrm{LOS,AOD}}\right) \\ F_{\mathrm{tx},s,\varphi}\left(\theta_{\mathrm{LOS,ZOD}}, \varphi_{\mathrm{LOS,AOD}}\right) \end{bmatrix} \\ & \cdot \exp\left(j2\pi\lambda_0^{-1}\left(\hat{\mathbf{r}}_{\mathrm{rx,LOS}}^{T} \cdot \overline{\mathbf{d}}_{\mathrm{rx},u}\right)\right) \cdot \exp\left(j2\pi\lambda_0^{-1}\left(\hat{\mathbf{r}}_{\mathrm{tx,LOS}}^{T} \cdot \overline{\mathbf{d}}_{\mathrm{tx},s}\right)\right) \\ & \cdot \exp\left(j2\pi\nu_{\mathrm{LOS}}t\right), \end{aligned} \tag{5}$$

where $\delta(\cdot)$ is Dirac's delta function. $F_{\mathrm{tx},s,\phi}$ and $F_{\mathrm{tx},s,\theta}$ are the antenna radiation patterns of transmit antenna s in the direction of the spherical basis vectors, $\hat{\boldsymbol{\varphi}}$ and $\hat{\boldsymbol{\theta}}$, respectively. $F_{\mathrm{rx},u,\phi}$ and $F_{\mathrm{rx},u,\theta}$ are the antenna radiation patterns of receive element u in the direction of the spherical basis vectors, $\hat{\boldsymbol{\varphi}}$ and $\hat{\boldsymbol{\theta}}$, respectively. $\overline{\mathbf{d}}_{\mathrm{rx},u}$ and $\overline{\mathbf{d}}_{\mathrm{tx},s}$ indicate the location vectors of the receive and transmit elements, respectively;

$$\hat{\mathbf{r}}_{\mathrm{tx},n,m} = \left[\sin\theta_{n,m,\mathrm{ZOD}}\cos\varphi_{n,m,\mathrm{AOD}} \quad \sin\theta_{n,m,\mathrm{ZOD}}\sin\varphi_{n,m,\mathrm{AOD}} \quad \cos\theta_{n,m,\mathrm{ZOD}}\right]^{T} \tag{6}$$

is the spherical unit vector with the elevation departure angle $\theta_{n,m,\mathrm{ZOD}}$ and the azimuth departure angle $\phi_{n,m,\mathrm{AOD}}$. Also $\hat{\mathbf{r}}_{\mathrm{rx},n,m}$ is the counterpart at the receive side. $\kappa_{n,m}$ is the cross-polarization power ratio. $\nu_{n,m}$ means the Doppler frequency component. K_R denotes the Ricean K-factor. λ_0 indicates the wavelength of the carrier frequency. $\{\Phi_{n,m}^{\theta\theta}, \Phi_{n,m}^{\theta\phi}, \Phi_{n,m}^{\phi\theta}, \Phi_{n,m}^{\phi\phi}\}$ are the random initial phases for the mth ray of the nth cluster and for four different polarizations combinations $\{\theta\theta, \theta\phi, \phi\theta, \phi\phi\}$. Due to space constraint, for more detailed description about the process of the 3D channel generation refer to [10].

2.3. Received Signal Model. Figure 2 depicts the multicell layout. Each hexagonal site is split into 3 cells. The BS in each cell is equipped with the URA. As depicted in Figure 1, the antenna array configuration comprises N_v antenna elements in the vertical direction and N_h antenna elements in the horizontal direction. So the total number of antennas is $N = N_h \times N_v$. Each user has N_r receiving antennas.

Here we just consider that the number of transmission spatial layers to each user is 1. The received signal vector $\mathbf{x}_j \in C^{(K\times N_r)\times 1}$ of the K coscheduled users in cell j can be expressed as

$$\mathbf{x}_j = \sqrt{\rho_f}\mathbf{H}_{jj}\mathbf{W}_j\mathbf{s}_j + \sum_{l=1, l\neq j}^{L} \sqrt{\rho_f}\mathbf{H}_{jl}\mathbf{W}_l\mathbf{s}_l + \mathbf{v}_j, \tag{7}$$

where $\mathbf{s}_j \in C^{K\times 1}$ is the vector of the transmitted signal. $\mathbf{H}_{jl} \in C^{(K\times N_r)\times N}$ is the channel matrix from the BS in cell l to the coscheduled users in cell j. ρ_f is the average transmit power. The second term $\sum_{l=1, l\neq j}^{L} \sqrt{\rho_f}\mathbf{H}_{jl}\mathbf{W}_l\mathbf{s}_l$ denotes the interference from the neighboring cells. $\mathbf{W}_j \in C^{N\times K}$ is the precoding matrix for the coscheduled users. $\mathbf{v}_j \sim CN(\mathbf{0}, \sigma^2\mathbf{I}_{K\times K})$ is the noise.

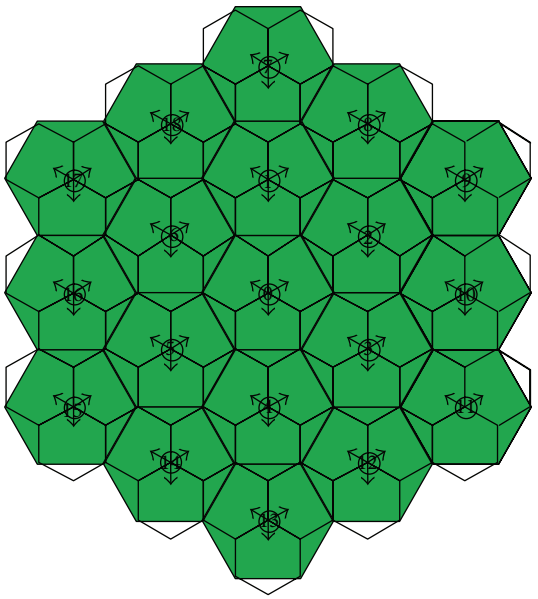

Figure 2: The cellular network of the downlink system.

3. 3D CSI Feedback Scheme

Based on the characteristics of URA, here we propose that the CSI for horizontal dimension and the CSI for vertical dimension are fed back separately. Assume that, based on the downlink pilot, each user achieves the perfect channel matrix. Then the user selects the appropriate precoding code words from the codebook for the horizontal and vertical domains, respectively.

Figure 3 depicts the cumulative distribution function (CDF) of zenith spread of departure angle (ZSD) and azimuth spread of departure angle (ASD) in 3D-UMa and 3D-UMi scenarios. In vertical plane, the angle spread (AS) is relatively smaller than that in horizontal plane in both scenarios.

Figure 4 shows the limited feedback model of 3D MIMO. Here we describe the limited feedback scheme for user k in cell j. The procedure of the code word selection for user k is as follows.

Step 1. Assume the transmitted antenna elements in the BS are rowwise indexed; the channel matrix from user k to the BS is $\mathbf{H}_k = [\mathbf{H}_{k1} \ \mathbf{H}_{k2} \ \cdots \ \mathbf{H}_{kN_v}] \in C^{N_r \times (N_v \times N_h)}$. $\mathbf{H}_{ki} \in C^{N_r \times N_h}$ $(i = 1, 2, \ldots, N_v)$ is the channel matrix between the ith row transmit antenna elements and user k. For convenience, here $\mathbf{H}_{ki}$ is called the horizontal channel. Calculate the average correlation matrix $\mathbf{R} \in C^{N_h \times N_h}$ for the N_v horizontal channels

$$\mathbf{R} = \frac{1}{N_v} \sum_{i=1}^{N_v} (\mathbf{H}_{ki})^H \mathbf{H}_{ki}. \tag{8}$$

Assume that the set of codebook for horizontal domain is $\mathbf{C}_h = \{\mathbf{c}_0^h, \mathbf{c}_1^h, \ldots, \mathbf{c}_{M_h-1}^h\}$, $M_h = 2^{B_h}$. So the optimal code word for the horizontal dimension can be selected as

$$\mathbf{w}_h = \mathbf{c}_m^h \in C^{N_h \times 1}, \quad m = \arg\max_{i=0,1,\ldots,M_h-1} \left| \mathbf{c}_i^h \mathbf{R} \mathbf{c}_i^{hH} \right|. \tag{9}$$

Step 2. When the antenna elements in the BS are columnwise indexed, the channel matrix between user k and the BS is $\mathbf{H}_k^* = [\mathbf{H}_{k1}^* \ \mathbf{H}_{k2}^* \ \cdots \ \mathbf{H}_{kN_h}^*] \in C^{N_r \times (N_h \cdot N_v)}$. $\mathbf{H}_{ki}^* \in C^{N_r \times N_v}$ $(i = 1, 2, \ldots, N_h)$ is the channel matrix from the ith column of antenna elements to user k. We call $\mathbf{H}_{ki}^*$ the vertical channel. So the average correlation matrix $\mathbf{R}^* \in C^{N_v \times N_v}$ for vertical domain is calculated as

$$\mathbf{R}^* = \frac{1}{N_h} \sum_{i=1}^{N_h} (\mathbf{H}_{ki}^*)^H \mathbf{H}_{ki}^*. \tag{10}$$

Assume that the set of codebook for vertical domain is $\mathbf{C}_v = \{\mathbf{c}_0^v, \mathbf{c}_1^v, \ldots, \mathbf{c}_{M_v-1}^v\}$, $(M_v = 2^{B_v})$. So the optimal code word for the vertical dimension is

$$\mathbf{w}_v = \mathbf{c}_m^v \in C^{N_v \times 1}, \quad m = \arg\max_{i=0,1,\ldots,M_v-1} \left| \mathbf{c}_i^v \mathbf{R}^* \mathbf{c}_i^{vH} \right|. \tag{11}$$

Step 3. The user k feeds back the code word indexes for horizontal and vertical domains separately to BS in cell j. In the BS, the 3D precoding vector $\mathbf{w}_k \in C^{(N_h \times N_v) \times 1}$ for channel matrix $\mathbf{H}_k$ is calculated as follows:

$$\mathbf{w}_k = \mathbf{w}_v \otimes \mathbf{w}_h, \tag{12}$$

where $\otimes$ denotes the Kronecker product.

For MU-MIMO, assume that the set of the scheduled users is $\mathbf{S} = \{s_1, s_2, \ldots, s_u\}$ in the BS. Based on the principle of maximizing the total capacity of the users, the BS selects the paired users from the set $\mathbf{S}$. In order to eliminate the interference of coscheduled users, the operation of zero forcing (ZF) is brought in to form the precoding matrix. The precoding matrix $\mathbf{W}_j$ in (7) can be expressed as

$$\mathbf{W}_j = \beta \mathbf{W} \left(\mathbf{W}^H \mathbf{W} \right)^{-1}, \quad \mathbf{W} = \left[\mathbf{w}_1 \ \mathbf{w}_2 \ \cdots \ \mathbf{w}_K \right], \tag{13}$$

where β is the normalization factor. K is the number of coscheduled users.

4. Proposed Codebook Design

The CSI can be fed back separately for the horizontal and vertical domains. In this paper, for a backward compatibility, we still exploit the existing codebook of LTE-Advanced for horizontal domain. Based on the ZoD distribution in 3D-UMa and 3D-UMi scenarios, we focus on the codebook design for the vertical dimension to balance the feedback overhead and the system performance.

4.1. ZoD Angle Quantization Codebook. Figure 5 depicts the ZoD of the user. ZoD is the angle measured between the zenith direction and the line connecting the user to the respective BS. Figure 6 presents the CDF of ZoD of all users in the cellular network under 3D-UMa and 3D-UMi scenarios, respectively.

We can see that the distribution range of ZoD mainly concentrates on 90° ~ 120° in 3D-UMa scenario and 70° ~ 110° in 3D-UMi scenario. Based on the distribution of the

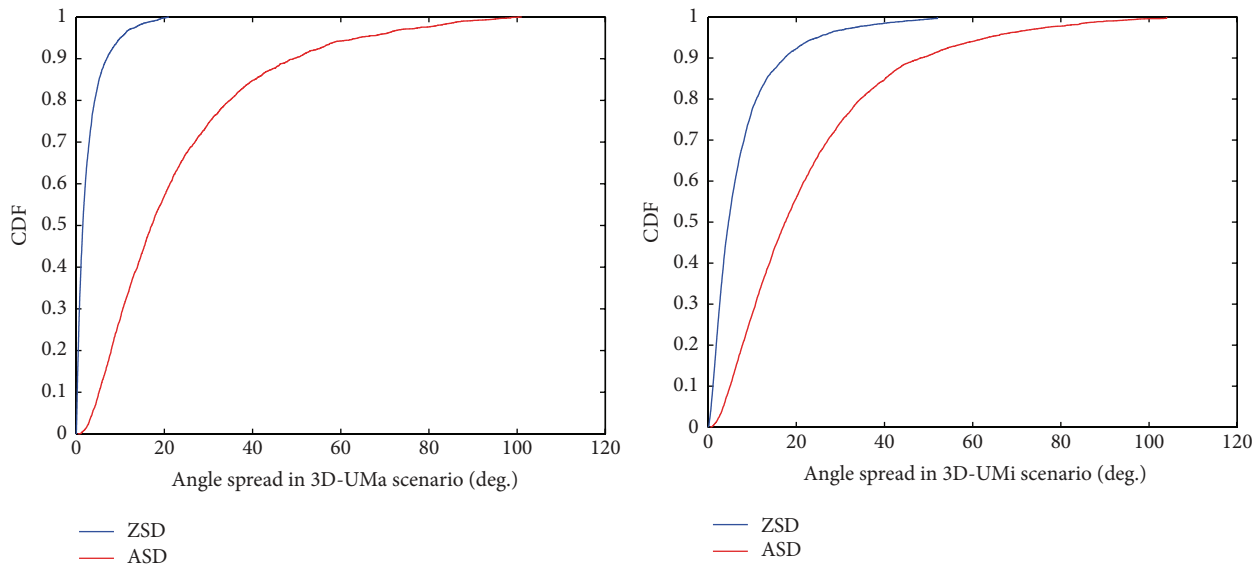

Figure 3: The CDF of ZSD in 3D-UMa and 3D-UMi scenarios.

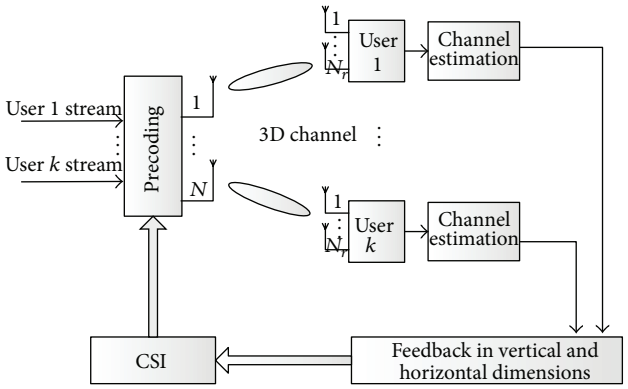

Figure 4: Limited feedback model of 3D MIMO.

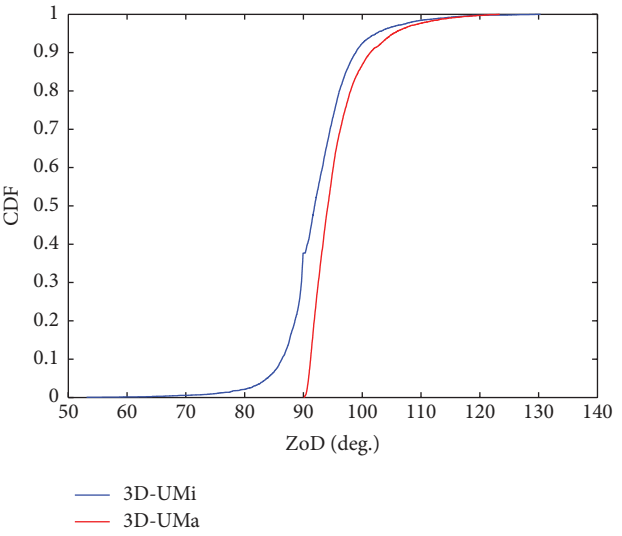

Figure 6: The CDF of users' ZoD in the cellular network under 3D-UMa scenario and 3D-UMi scenario.

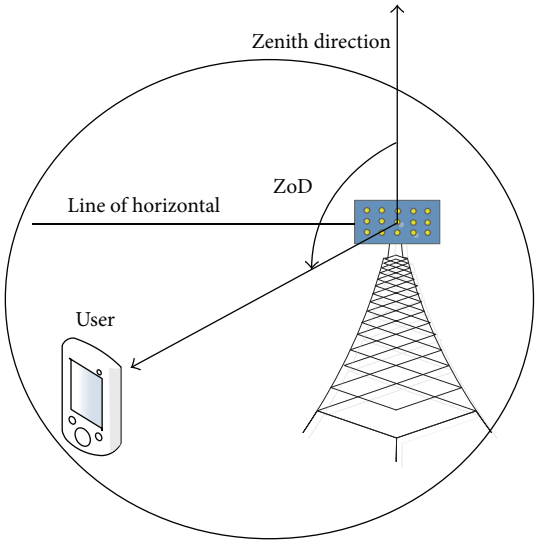

Figure 5: The definition of ZoD.

ZoD, we propose angle quantization codebook set $\mathbf{C}_v = \{\mathbf{c}_0^v, \mathbf{c}_1^v, \ldots, \mathbf{c}_{M_v-1}^v\}$ $(M_v = 2^{B_v})$ for the vertical domain. The code word $\mathbf{c}_i^v$ in $\mathbf{C}_v$ is expressed as

$$\mathbf{c}_i^v = \left[w_0^i \;\; w_2^i \;\; \cdots \;\; w_{N_v-1}^i\right]^T,$$
$$w_n^i = \frac{1}{\sqrt{N_v}} \exp\left[-j\frac{2\pi}{\lambda} n d_v \cos\left(\theta_i\right)\right], \tag{14}$$

where $i = 0, 1, \ldots, 2^{B_v} - 1$ is the index of the code word. N_v is the number of antennas in vertical direction. θ_i is the quantized angle value. B_v is the codebook size (in bits). d_v is the space between the vertical antenna elements. λ is the carrier wavelength.

For small ZSD in the vertical domain, increasing the codebook size B of the angle quantization codebook can improve the system performance; while the AS or the codebook size B is large enough, increasing the codebook size B does not work. This will be proved in Appendix.

Considering the feedback overhead and system performance, we assign B_v to 4, 3, 2, and 1 to evaluate the system performance. The details of the codebook design are listed as follows.

4.1.1. Codebook for 3D-UMa Scenario

Codebook 1-4. Consider $B_v = 4$ and uniform quantization in the angle range $90^\circ \sim 120^\circ$.

Codebook 1-3-a. Consider $B_v = 3$ and uniform quantization in the angle range $90^\circ \sim 120^\circ$.

The uniform quantization can be calculated as

$$\theta_i = \left[90 + \frac{120 - 90}{2^{B_v}} \times i\right]. \tag{15}$$

Also we can select the angles nonuniformly based on the CDF of the users' ZoD. Codebooks 1-3-b, 1-2, 1-1-a, 1-1-b, and 1-1-c select the angles which account for a large percentage of the ZoD distribution under 3D-UMa scenario in Figure 6 to construct the angle set.

Codebook 1-3-b. Consider $B_v = 3$ and $\theta_i \in \boldsymbol{\theta}_{1\text{-}3\text{-}b} = \{92, 94, 96, 98, 100, 102, 107, 113\}$.

Codebook 1-2. Consider $B_v = 2$ and $\theta_i \in \boldsymbol{\theta}_{1\text{-}2} = \{91, 95, 99, 102\}$.

Codebook 1-1-a. Consider $B_v = 1$ and $\theta_i \in \boldsymbol{\theta}_{1\text{-}1\text{-}a} = \{95, 102\}$.

Codebook 1-1-b. Consider $B_v = 1$ and $\theta_i \in \boldsymbol{\theta}_{1\text{-}1\text{-}b} = \{95, 99\}$.

Codebook 1-1-c. Consider $B_v = 1$ and $\theta_i \in \boldsymbol{\theta}_{1\text{-}1\text{-}c} = \{93, 97\}$.

4.1.2. Codebook for 3D-UMi Scenario

Codebook 2-4. Consider $B_v = 4$ and uniform quantization in the angle range $70^\circ \sim 110^\circ$.

Codebook 2-3-a. Consider $B_v = 3$ and uniform quantization in the angle range $70^\circ \sim 110^\circ$.

The uniform quantization of θ_i can be calculated as

$$\theta_i = \left[70 + \frac{110 - 70}{2^{B}} \times i\right]. \tag{16}$$

Codebook 2-3-b. Consider $B_v = 3$ and $\theta_i \in \boldsymbol{\theta}_{2\text{-}3\text{-}b} = \{75, 80, 85, 90, 93, 95, 102, 107\}$.

Codebook 2-2-a. Consider $B_v = 2$ and $\theta_i \in \boldsymbol{\theta}_{2\text{-}2\text{-}a} = \{85, 90, 95, 102\}$.

Codebook 2-2-b. Consider $B_v = 2$ and $\theta_i \in \boldsymbol{\theta}_{2\text{-}2\text{-}b} = \{85, 89, 93, 98\}$.

Codebook 2-1-a. Consider $B_v = 1$ and $\theta_i \in \boldsymbol{\theta}_{2\text{-}1\text{-}a} = \{90, 102\}$.

Codebook 2-1-b. Consider $B_v = 1$ and $\theta_i \in \boldsymbol{\theta}_{2\text{-}1\text{-}b} = \{90, 95\}$.

Codebook 2-1-c. Consider $B_v = 1$ and $\theta_i \in \boldsymbol{\theta}_{2\text{-}1\text{-}c} = \{89, 98\}$.

Also, in codebooks 2-3-b, 2-2-a, 2-2-b, 2-1-a, 2-1-b, and 2-1-c, the angle set is made up of the angles which account for a large percentage of the ZoD distribution under 3D-UMi scenario in Figure 6.

4.2. Sampling DFT Codebook. Discrete Fourier Transform-(DFT-) based codebook is favored by LTE for its simplicity. And in [19], it reveals that DFT-based codebook is effective for small AS. The simulation results in Section 5 reveal that 3-bit angle quantization codebook for 3D-UMa and 3D-UMi scenarios can guarantee the system performance. To make full use of the orthogonality of the DFT-based codebook, here we select code words from 5-bit 32-DFT codebook to construct 3-bit codebook set for vertical domain.

The code word $\mathbf{w}_p$ of the 5-bit 32-DFT codebook set $\mathbf{W}_{\text{DFT}} = \{\mathbf{w}_0 \ \cdots \ \mathbf{w}_p \ \cdots \ \mathbf{w}_{31}\}$ is expressed as

$$\begin{aligned} \mathbf{w}_p &= \left[w_0^p \ \ w_2^p \ \ \cdots \ \ w_{N_v-1}^p\right]^T, \\ w_m^p &= \frac{1}{\sqrt{N_v}} \exp\left(-j2\pi \frac{mp}{32}\right), \end{aligned} \tag{17}$$

where $m = 0, 1, \ldots, N_v - 1$. $p = 0, 1, 2, \ldots, 31$ is the index of code word.

To select 8 code words from $\mathbf{W}_{\text{DFT}}$ and construct 3-bit codebook, we need to calculate the corresponding beam directions of 32-DFT codebook through the expression

$$\exp\left(-j2\pi \frac{mp}{32}\right) = \exp\left(-j2\pi \frac{md_v}{\lambda} \cos\theta_p\right). \tag{18}$$

Here we just cope with the condition in which $d_v = 0.5\lambda$. Calculated by (18), the set of the beam direction θ_p corresponding to the code word in $\mathbf{W}_{\text{DFT}}$ sorted by p from 0 to 31 is

$$\begin{aligned} \boldsymbol{\Theta}_p = \{&90, 86.42, 82.82, 79.19, 75.52, 71.79, 67.98, \\ &64.06, 60, 55.77, 51.32, 46.57, 41.41, 35.66, 28.96, \\ &20.36, 180, 159.64, 151.05, 144.34, 138.59, 133.43, \\ &128.68, 124.23, 120, 115.94, 112.02, 108.21, 104.48, \\ &100.81, 97.18, 93.58\}. \end{aligned} \tag{19}$$

4.2.1. DFT-Based Codebook for 3D-UMa Scenario. Here we utilize the construction of codebook 1-3-c as an example to show how to select code word elements from $\mathbf{W}_{\text{DFT}}$ to generate the 3-bit 32-DFT codebook. The angle set corresponding to codebook 1-3-a is $\boldsymbol{\theta}_{1\text{-}3\text{-}a} = \{90, 93.75, 97.5, 101.25, 105, 108.75, 112.5, 116.25\}$. Based on the angle set $\boldsymbol{\theta}_{1\text{-}3\text{-}a}$, we select angle elements from $\boldsymbol{\Theta}_p$ to construct angle set $\boldsymbol{\theta}_{1\text{-}3\text{-}c}$. The angle element selection from $\boldsymbol{\Theta}_p$ follows the principles as below:

(1) The elements in $\boldsymbol{\theta}_{1\text{-}3\text{-}c}$ are approximately equal to the elements in set $\boldsymbol{\theta}_{1\text{-}3\text{-}a}$.

(2) The elements in $\boldsymbol{\theta}_{1\text{-}3\text{-}a}$ are sorted in ascending order. So the element values in $\boldsymbol{\theta}_{1\text{-}3\text{-}c}$ corresponding to the elements in $\boldsymbol{\theta}_{1\text{-}3\text{-}a}$ are also sorted in ascending order. Also for 3D-UMa scenario, the range of angle values is restricted to $90^\circ \sim 120^\circ$.

So following the principles, corresponding to the set $\boldsymbol{\theta}_{1\text{-}3\text{-}a}$, we can get $\boldsymbol{\theta}_{1\text{-}3\text{-}c} = \{90, 93.58, 97.18, 100.81, 104.48, 108.21, 112.02, 115.94\}$ from $\boldsymbol{\Theta}_p$. The index set corresponding to the angle elements of $\boldsymbol{\theta}_{1\text{-}3\text{-}c}$ in $\boldsymbol{\Theta}_p$ is $\{0, 31, 30, 29, 28, 27, 26, 25\}$. So based on the index set, we select code words from $\mathbf{W}_{\text{DFT}}$ to construct the codebook 1-3-c:

$$\mathbf{W}_{1\text{-}3\text{-}c} = \{\mathbf{w}_0 \ \ \mathbf{w}_{31} \ \ \mathbf{w}_{30} \ \ \mathbf{w}_{29} \ \ \mathbf{w}_{28} \ \ \mathbf{w}_{27} \ \ \mathbf{w}_{26} \ \ \mathbf{w}_{25}\}. \quad (20)$$

Via the same method, we can construct the codebook $\mathbf{W}_{1\text{-}3\text{-}d}$ based on codebook 1-3-b. According to the angle set $\boldsymbol{\theta}_{1\text{-}3\text{-}b} = \{92, 94, 96, 98, 100, 102, 107, 113\}$ of codebook 1-3-b, the angle set $\boldsymbol{\theta}_{1\text{-}3\text{-}d}$ is $\{90, 93.58, 97.18, 100.81, 104.48, 108.21, 112.02, 115.94\}$. Through the index set corresponding to the angle elements of $\boldsymbol{\theta}_{1\text{-}3\text{-}d}$ from $\boldsymbol{\Theta}_p$, we can get the code words in $\mathbf{W}_{\text{DFT}}$. So codebook 1-3-d can be expressed as

$$\mathbf{W}_{1\text{-}3\text{-}d} = \{\mathbf{w}_0 \ \ \mathbf{w}_{31} \ \ \mathbf{w}_{30} \ \ \mathbf{w}_{29} \ \ \mathbf{w}_{28} \ \ \mathbf{w}_{27} \ \ \mathbf{w}_{26} \ \ \mathbf{w}_{25}\}. \quad (21)$$

Because the range of ZoD under 3D-UMa scenario is small, the 3-bit DFT codebook 1-3-c corresponding to codebook 1-3-a and codebook 1-3-d corresponding to codebook 1-3-b are the same.

4.2.2. DFT-Based Codebook for 3D-UMi Scenario. Here we will adopt the same method above to design the 3-bit 32-DFT codebook for 3D-UMi scenario.

The angle set of codebook 2-3-a is $\boldsymbol{\theta}_{2\text{-}3\text{-}a} = \{70, 75, 80, 85, 90, 95, 100, 105\}$. So the corresponding angle subset from the set $\boldsymbol{\Theta}_p$ is $\boldsymbol{\theta}_{2\text{-}3\text{-}c} = \{71.79, 75.52, 79.19, 86.42, 90, 93.58, 100.81, 104.48\}$. Based on the indexes of the angle elements of $\boldsymbol{\theta}_{2\text{-}3\text{-}c}$ in $\boldsymbol{\Theta}_p$, we can select code words from $\mathbf{W}_{\text{DFT}}$ to construct codebook 2-3-c:

$$\mathbf{W}_{2\text{-}3\text{-}c} = \{\mathbf{w}_5 \ \ \mathbf{w}_4 \ \ \mathbf{w}_3 \ \ \mathbf{w}_1 \ \ \mathbf{w}_0 \ \ \mathbf{w}_{31} \ \ \mathbf{w}_{29} \ \ \mathbf{w}_{28}\}. \quad (22)$$

$\boldsymbol{\theta}_{2\text{-}3\text{-}b} = \{75, 80, 85, 90, 93, 95, 102, 107\}$ is the angle set of codebook 2-3-b. The corresponding angle set from $\boldsymbol{\Theta}_p$ is $\boldsymbol{\theta}_{2\text{-}3\text{-}d} = \{75.52, 82.82, 86.42, 90, 93.58, 97.18, 100.81, 108.21\}$. So we obtain codebook 2-3-d:

$$\mathbf{W}_{2\text{-}3\text{-}d} = \{\mathbf{w}_4 \ \ \mathbf{w}_2 \ \ \mathbf{w}_1 \ \ \mathbf{w}_0 \ \ \mathbf{w}_{31} \ \ \mathbf{w}_{30} \ \ \mathbf{w}_{29} \ \ \mathbf{w}_{27}\}. \quad (23)$$

5. Numerical Results

To evaluate the proposed scheme and codebook design, the system-level simulation is performed. In the simulation, the cellular network layout adopts wrap-round technique. As depicted in Figure 2, there are 19 hexagonal sites each with 3 cells in horizontal domain. So the cellular network consists of 57 cells. And each cell accommodates 10 active users. For the generation of 3D channel model refer to [10]. For simplicity, detailed simulation parameters are listed in Table 1. The configuration of the 2D planar uniformly spaced antenna array in the BS can be represented by (M, N, P). M is the number of antenna elements with the same polarization in each column. N is the number of columns. P is number of polarization dimensions. Each user is equipped with 2 antennas; namely, $N_r = 2$.

Table 1: Simulation parameters configuration.

Parameters	Settings
Bandwidth	10 MHz
Antenna element interval	0.5λ both in horizontal and vertical directions
Carrier frequency	2 GHz
The number of users per cell	10
User distribution	Refer to [10]
User speed	3 km/h
Traffic model	Full buffer
Schedule	Proportional fair
Channel estimation	Ideal
Receiver	MMSE
HARQ	The maximal number of retransmissions is 4
Wrapping method	Geographical distance based

5.1. Separate CSI Feedback for Horizontal and Vertical Domains. To make a comparison with the proposed scheme, we introduce the method in [18] as the benchmark scheme which also proposes a separation of the vertical and horizontal domains. In this subsection, the antennas array configuration is (8, 8, 1); namely, $N_v = N_h = 8$, and we adopt the copolarized antenna array. The proposed scheme utilizes the same 5-bit 32-DFT codebook for horizontal and vertical dimensions, respectively. In the benchmark scheme, assume that it transmits one stream in horizontal domain and one stream in vertical domain, respectively. Here the code word for the benchmark scheme in two domains is the 64×1 vector. We adopt the method in [16] to generate the codebook for the benchmark scheme. It utilizes two 5-bit 32-DFT codebooks to generate the 10-bit codebook by the Kronecker product. Each code word is a 64×1 vector.

Figure 7 shows the simulation results of the two schemes in single-user MIMO system under 3D-UMa and 3D-UMi scenarios. We can see that the performance of the proposed scheme has a slight decrease compared to the benchmark scheme. When the horizontal and vertical domains utilize the same codebook set, the benchmark scheme needs to store 2^{10} code words and the feedback overhead for each domain is 10 bits while the proposed scheme just needs to store 2^5 code words and the feedback overhead for each domain is 5 bits. What is more, quantizing the 8×1 vector in the proposed scheme has a lower complexity relative to quantizing the 64×1 vector in the benchmark scheme. Though there is a slight performance degradation, the proposed scheme reduced the storage requirement, feedback overhead, and search complexity compared to the benchmark scheme.

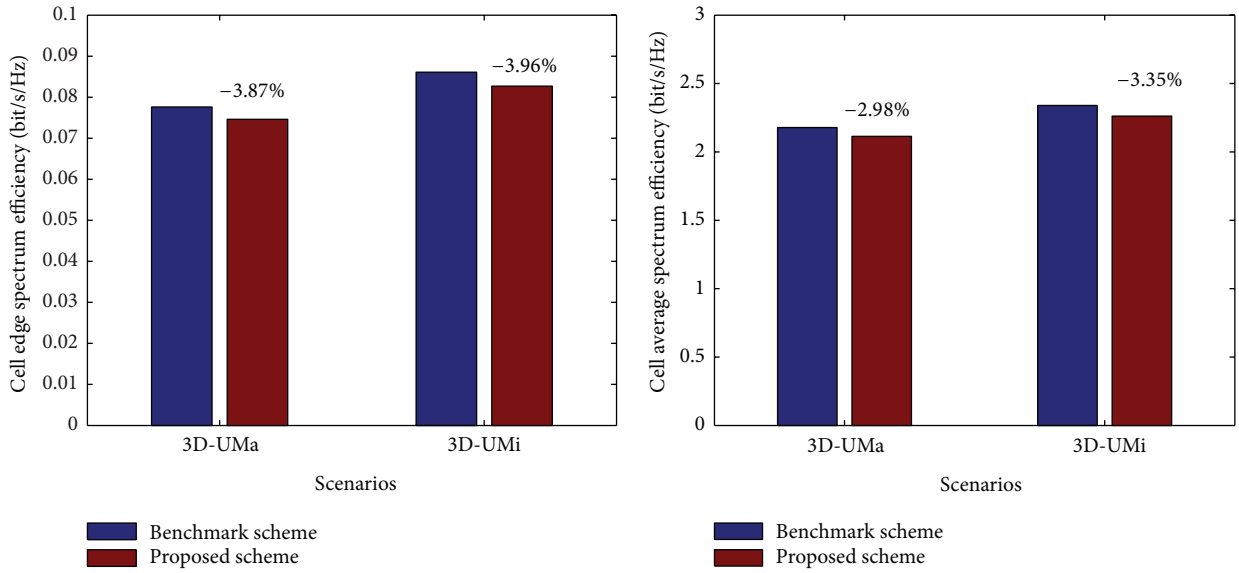

Figure 7: The system-level simulation results of the proposed feedback scheme.

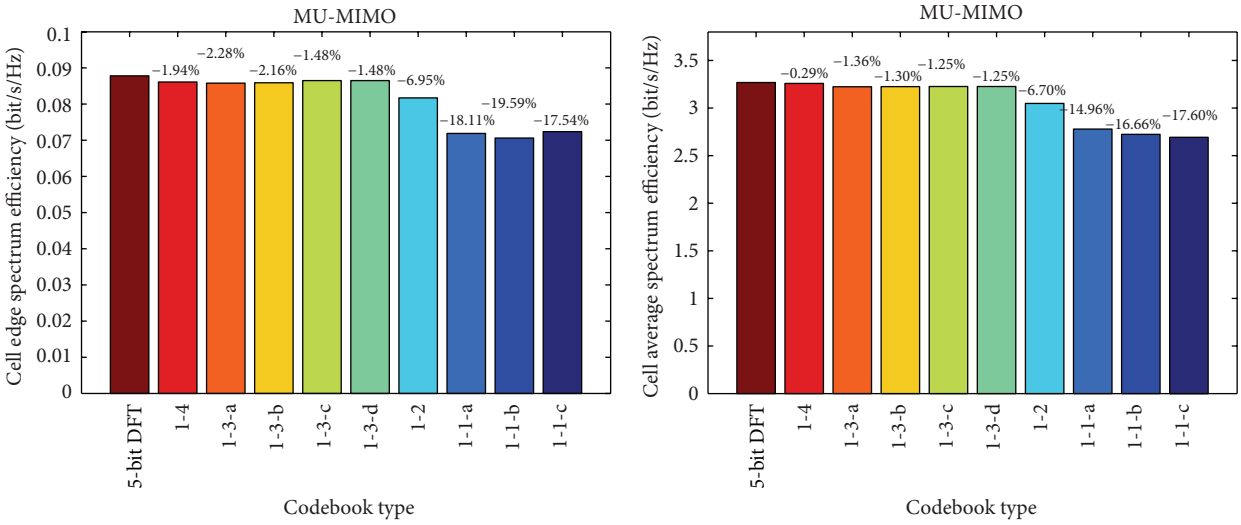

Figure 8: Simulation results of the codebooks for the vertical domain under 3D-UMa scenario.

5.2. Codebook Design for the Vertical Domain. Dual polarization can not only save antenna space but also provide diversity gain and rich scattering for more degrees of freedom. In this subsection, the cross-polarized antenna array is adopted. The antenna array configuration is (10, 4, 2); namely, $N_v = 10$ and $N_h = 4 \times 2 = 8$. And we adopt $\pm 45^\circ$ cross-polarized antennas. In the horizontal domain, the 8Tx codebook of LTE-Advanced which is a double codebook design and is appropriate for cross-polarized array is utilized [20]. In the vertical domain, the proposed codebooks in Section 4 are evaluated. Figures 8 and 9 show the simulation results in MU-MIMO system under 3D-UMa and 3D-UMi scenarios. The maximal number of coscheduled users is 4.

For 3D-UMa scenario, relative to the performance of the 5-bit 32-DFT codebook in vertical domain, the performances of codebooks 1-4, 1-3-a, 1-3-b, 1-3-c, and 1-3-d decline slightly as shown in Figure 8. The cell average spectrum efficiency of the 2-bit codebook 1-2 goes down by 6.70% and the cell edge spectrum efficiency decreases by 6.95%. The feedback overhead reduces 3 bits from 5 bits to 2 bits and the loss of the system performance is acceptable. However, the performance of 1-bit codebook such as 1-1-a, 1-1-b, and 1-1-c has a sharp degradation.

For 3D-UMi scenario, Figure 9 shows that, considering the feedback overhead and the performance, 3-bit codebooks including codebooks 2-3-a, 2-3-b, 2-3-c, and 2-3-d are appropriate and acceptable relative to 5-bit 32-DFT codebook. But the 2-bit codebooks perform poorly. Relative to the 5-bit 32-DFT codebook, the cell average spectrum efficiency of codebooks 2-2-a and 2-2-b decreases by about 12% and the cell edge spectrum efficiency decreases by about 18%.

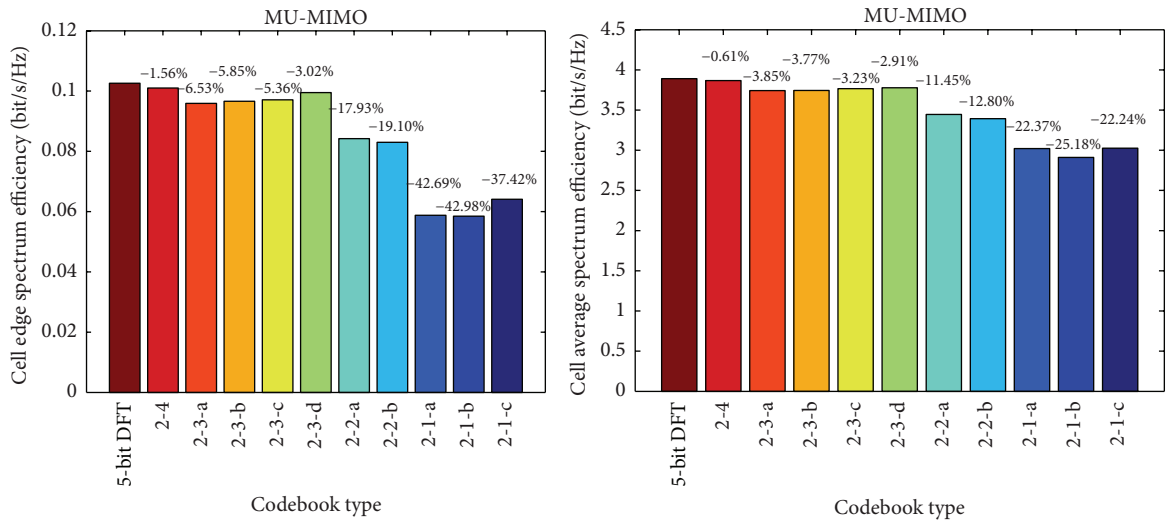

Figure 9: Simulation results of the codebooks for the vertical domain under 3D-UMi scenario.

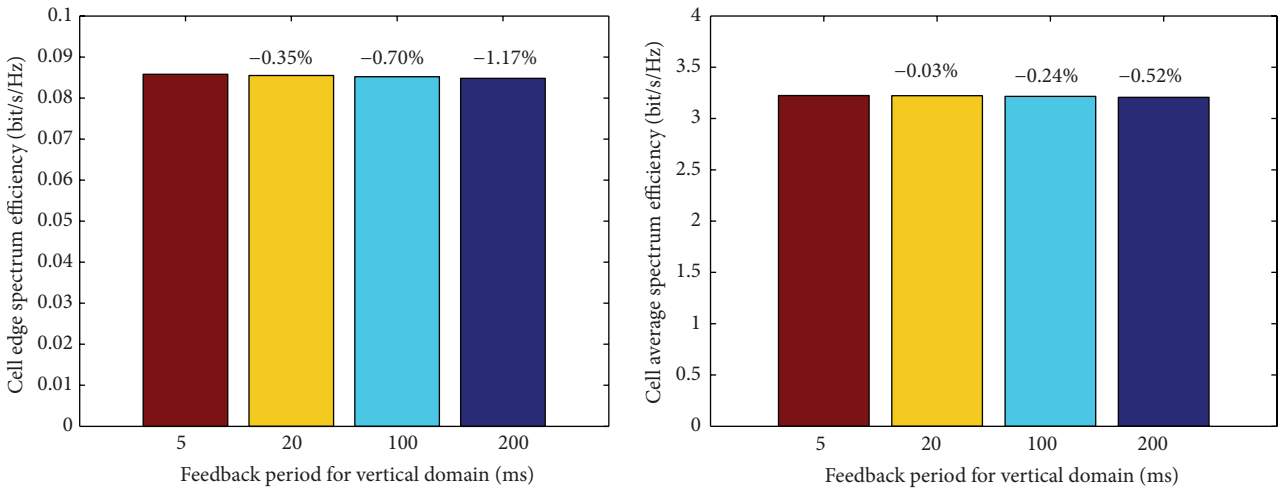

Figure 10: Feedback period for vertical domain with different values in 3D-UMa scenario.

The performance of the 1-bit codebooks including codebooks 2-1-a, 2-1-b, and 2-1-c drops drastically.

The 4-bit codebooks, such as codebooks 1-4 and 2-4, behave well for 3D-UMa and 3D-UMi scenarios. To reduce the feedback overhead, the 3-bit codebook is viable and worth recommending for 3D-UMi scenario while for 3D-UMa scenario 2-bit codebook tends to be attractive. The reason is that the distribution range of ZoD in 3D-UMi scenario is larger than that in 3D-UMa scenario.

Also we can see the nonuniform quantization angle codebook outperforms slightly the uniform quantization angle codebook. Because the ZoD distribution range is small in both scenarios, the performances of the two types of codebooks are close.

Relative to the corresponding angle quantization codebooks, the 3-bit DFT-based codebooks achieve a slight improvement in performance. In general, the performances of the 3-bit DFT-based codebook and the corresponding angle quantization codebook are also close because of the small ZoD distribution range.

5.3. The Extension of Feedback Period for Vertical Domain. In the simulations above, the feedback periods for the horizontal and vertical domains are both 5 ms. In practice, the CSI feedback for horizontal domain and vertical domain can be operated separately. So in this subsection, we study the situation of different feedback periods for the two domains. Here we let the feedback period for horizontal domain remain 5 ms and let the feedback period for vertical domain vary from 5 ms to 20 ms, 100 ms, and 200 ms. In the simulation, codebook 1-3-a is used for 3D-UMa scenario and codebook 2-3-a is used for 3D-UMi scenario for the vertical domain. The antenna array configuration is the same to the configuration in Section 5.2.

From Figures 10 and 11, we can see that, relative to the performance of the feedback period 5 ms, the cell average

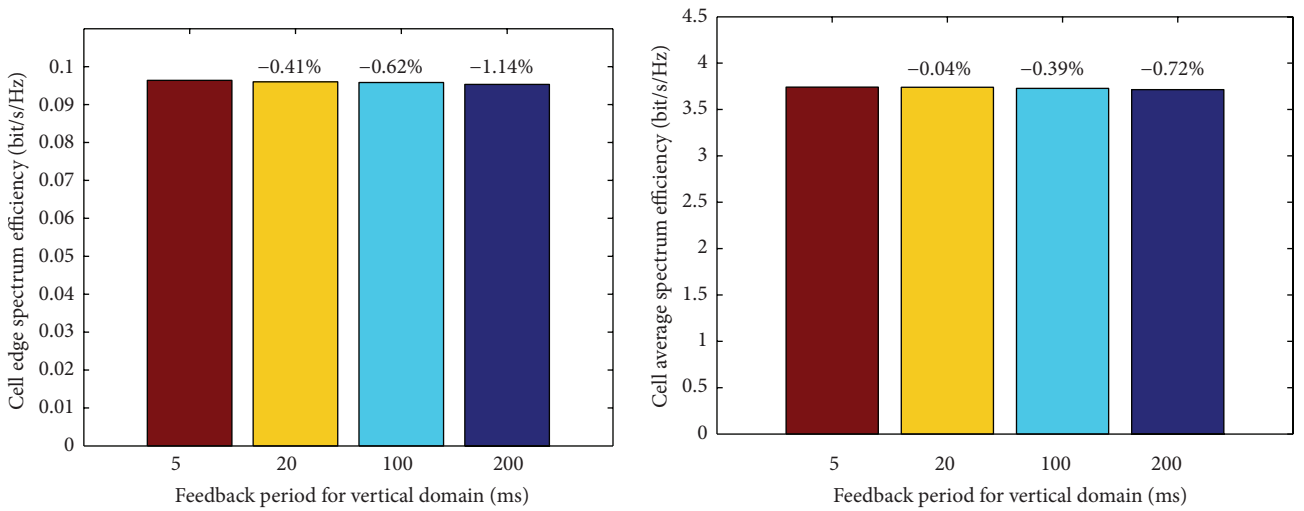

Figure 11: Feedback period for vertical domain with different values in 3D-UMi scenario.

spectrum efficiency and cell edge spectrum efficiency decline slightly as the feedback period for vertical domain extends. This is because the ZSD is small in vertical domain as depicted in Figure 3 and the speed of users in vertical direction is very slow. This means that the feedback period for the vertical domain can be extended appropriately to decrease the feedback overhead.

6. Conclusion

In this paper, we study the separate feedback scheme for 3D massive MIMO. It can reduce the feedback overhead, search complexity, and the storage of the code words. Based on the feature of 3D-UMa scenario and 3D-UMi scenario, the angle quantization codebooks for vertical domain are proposed. Also the 3-bit DFT-based codebook selected from 32-DFT codebook is recommended. In the end, corresponding to the feedback separation for 3D MIMO in the two domains, we reveal that the feedback period for vertical domain can be extended more in order to decrease the feedback overhead.

Appendix

In [21], the authors analyse the per user rate loss led by utilizing DFT codebook. Here based on the method we investigate the per user rate loss led by angle quantization codebook in vertical domain. Because the angle quantization codebook is designed for vertical domain, for simplicity, we just consider the channel model for ULA which is vertically positioned. Figure 12 presents the channel vector of user k consisting of N uncorrelated subpaths. The channel can be expressed as

$$\mathbf{h}_k = \sum_{n=1}^{N} a_{k,n}\mathbf{u}\left(\beta_{k,n}\right) = \mathbf{U}_k\mathbf{a}_k, \tag{A.1}$$

where $a_{k,n}$ is the subpaths gain. $\mathbf{u}(\beta_{k,n}) = \left[1 \;\; e^{-j2\pi\beta_{k,n}} \;\; \cdots \;\; e^{-j2\pi(\mathrm{M}-1)\beta_{k,n}}\right]^T$ is the steering vector. M is the number of antenna elements. One has $\theta_{k,n} \in [0,\pi]$ and $\beta_{k,n} = \mathrm{mod}((d_v/\lambda)\cos\theta_{k,n}, 1) \in [-1,1]$. $a_{k,n}$ is independent of $\beta_{k,n}$. d_v is antenna spacing distance in vertical direction. λ is the wavelength. $\theta_{k,n}$ is the angle of subpath n with respect to the zenith direction. $\mathbf{U}_k = \left[\mathbf{u}(\beta_{k,1}) \;\cdots\; \mathbf{u}(\beta_{k,N})\right]$ is the direction matrix. $\mathbf{a}_k = \left[a_{k,1} \;\cdots\; a_{k,N}\right]^T$ is the gain vector. Assume that $E(\|\mathbf{h}_k\|^2) = E(M\sum_{n=1}^{N}|a_{k,n}|^2) = 1$.

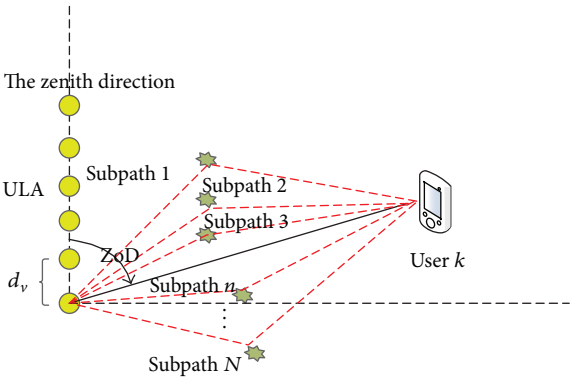

Figure 12: The channel model with N subpaths.

For simplicity, here we just analyse the uniform quantization angle codebook. The ith code word in a B-bit codebook is

$$\begin{aligned}\mathbf{c}\left(\phi_i\right) &= \frac{1}{\sqrt{M}}\left[1 \;\; e^{-j2\pi\phi_i} \;\; \cdots \;\; e^{-j2\pi(M-1)\phi_i}\right]^T,\\ \phi_i &= \mathrm{mod}\left(\frac{d_v}{\lambda}\cos\left(\theta_i\right), 1\right)\\ &= \mathrm{mod}\left(\frac{d_v}{\lambda}\cos\left(\theta_0 + i\cdot\frac{\theta_1-\theta_0}{2^B}\right), 1\right)\\ &\in [-1,1],\end{aligned} \tag{A.2}$$

where $[\theta_0,\theta_1]$ is the distribution range of the users' ZoD.

Because formula (A.2) is the same to formula (4) in [21] in form, the conclusion of DFT codebook can be applicable to the angle quantization codebook. So we can get the conclusions from [21] as follows.

Define $\overline{\beta_k} = \arg\min_{\phi_i} \sum_n^N |a_{k,n}|^2 (\beta_{k,n} - \phi_i)^2$. When the AS in elevation domain is small, $|\overline{\beta_k} - \beta_{k,n}| < 2^{-B}$ can be satisfied. The gap between the rate with perfect CSI and the rate with limited feedback

$$\Delta R \leq \log_2 \left(1 + \frac{P(M-1)}{M} c_1 2^{-2B} + c_0\right), \quad (A.3)$$

where c_0 and c_1 are constants. P is transmit power of the BS.

This means that we can increase the codebook size B to improve the system performance when AS is small. When B goes to infinity, ϕ_i approaches a continuous value; the rate loss is more tightly upper bounded by

$$\Delta R \leq \log_2 \left(1 + \frac{P(M-1)}{M} \left(c_1 E\left\{\sigma_k^2\right\} + c_0\right)\right), \quad (A.4)$$

where $\overline{\beta_k} = \sum_n |a_{k,n}|^2 \beta_{k,n} / \sum_n |a_{k,n}|^2$ and $\sigma_k^2 = \sum_n |a_{k,n}|^2 (\beta_{k,n} - \overline{\beta_k})^2 / \sum_n |a_{k,n}|^2$.

This means that increasing the codebook size cannot improve the sum rate in this situation.

Conflict of Interests

The authors declare that there is no conflict of interests regarding the publication of this paper.

Acknowledgments

This research has been supported by 863 Project of China (no. 2014AA01A705) and the State Key Laboratory of Wireless Mobile Communication of China Academy of Telecommunication Technology (no. 2007DQ305156).

References

[1] E. G. Larsson, O. Edfors, F. Tufvesson, and T. L. Marzetta, "Massive MIMO for next generation wireless systems," *IEEE Communications Magazine*, vol. 52, no. 2, pp. 186–195, 2014.

[2] F. Ruuek, D. Persson, E. G. Lau et al., "Scaling Up MIMO: opportunities and challenges with very large arrays," *IEEE Signal Processing Magazine*, vol. 30, no. 1, pp. 40–60, 2013.

[3] X. Lu, A. Tölli, O. Piirainen, M. Juntti, and W. Li, "Comparison of antenna arrays in a 3-D multiuser multicell network," in *Proceedings of the IEEE International Conference on Communications (ICC '11)*, pp. 1–6, June 2011.

[4] 3GPP RP-141644, "New SID Proposal: Study on Elevation Beamforming/Full-Dimension (FD) MIMO for LTE," Samsung, Nokia Networks, 2014.

[5] Y. Xie, S. Jin, J. Wang, Y. Zhu, X. Gao, and Y. Huang, "A limited feedback scheme for 3D multiuser MIMO based on Kronecker product codebook," in *Proceedings of the IEEE 24th Annual International Symposium on Personal, Indoor, and Mobile Radio Communications (PIMRC '13)*, pp. 1130–1135, September 2013.

[6] X. Cheng, B. Yu, L. Yang et al., "Communicating in the real world: 3D MIMO," *IEEE Wireless Communications*, vol. 21, no. 4, pp. 136–144, 2014.

[7] Y. Li, X. Ji, M. Peng, Y. Li, and C. Huang, "An enhanced beamforming algorithm for three dimensional MIMO in LTE-advanced networks," in *Proceedings of the International Conference on Wireless Communications and Signal Processing (WCSP '13)*, pp. 1–5, October 2013.

[8] A. Kammoun, H. Khanfir, Z. Altman, M. Debbah, and M. Kamoun, "Preliminary results on 3D channel modeling: from theory to standardization," *IEEE Journal on Selected Areas in Communications*, vol. 32, no. 6, pp. 1219–1229, 2014.

[9] M. Jiang, M. Hosseinian, M.-I. Lee, and J. Stern-Berkowitz, "3D channel model extensions and characteristics study for future wireless systems," in *Proceedings of the IEEE 24th Annual International Symposium on Personal, Indoor, and Mobile Radio Communications (PIMRC '13)*, pp. 41–46, September 2013.

[10] *Study on 3D Channel Model for LTE (Release 12)*, 3GPP TR 36.873 V12.1.0, 2015.

[11] Y.-G. Lim and C.-B. Chae, "Compressed channel feedback for correlated massive MIMO systems," in *Proceedings of the IEEE International Conference on Communications Workshops (ICC '14)*, pp. 360–364, June 2014.

[12] J. Choi, Z. Chance, and D. J. Love, "Noncoherent trellis-coded quantization for massive MIMO limited feedback beamforming," in *Proceedings of the 47th Annual Conference on Information Sciences and Systems (CISS '13)*, pp. 1–6, Baltimore, Md, USA, March 2013.

[13] S. Bazzi, G. Dietl, and W. Utschick, "Subspace precoding with limited feedback for the massive MIMO interference channel," in *Proceedings of the IEEE 8th Sensor Array and Multichannel Signal Processing Workshop (SAM '14)*, pp. 277–280, IEEE, A Coruña, Spain, June 2014.

[14] H. Wang, W. Wang, and Z. Zhang, "On the design of hybrid limited feedback for massive MIMO systems," in *Proceedings of the 1st IEEE International Conference on Communications (ICC '14)*, pp. 4795–4800, June 2014.

[15] H. Noh, Y. Kim, J. Lee, and C. Lee, "Codebook design of generalized space shift keying for FDD massive MIMO systems in spatially correlated channels," *IEEE Transactions on Vehicular Technology*, vol. 64, no. 2, pp. 513–523, 2015.

[16] X. Su, J. Zeng, J. Li et al., "Limited feedback precoding for massive MIMO," *International Journal of Antennas and Propagation*, vol. 2013, Article ID 416352, 9 pages, 2013.

[17] D. Han, W. Yang, Y. Peng, and Y. Zhu, "A limited feedback transmission scheme based on MS compensation in the 3D MIMO system," *China Communications*, vol. 11, no. 14, pp. 102–110, 2014.

[18] Y. Yuan, Y. Wang, W. Zhang, and F. Peng, "Separate horizontal & vertical codebook based 3D MIMO beamforming scheme in LTE-A networks," in *Proceedings of the IEEE 78th Vehicular Technology Conference (VTC '13)*, pp. 1–5, September 2013.

[19] D. Yang, L.-L. Yang, and L. Hanzo, "DFT-based beamforming weight-vector codebook design for spatially correlated channels in the unitary precoding aided multiuser downlink," in *Proceedings of the IEEE International Conference on Communications (ICC '10)*, pp. 1–5, May 2010.

[20] *Physical Layer Procedures (Release 12)*, 3GPP, TS 36.213 v12.5.0, 2015.

[21] F. Yuan, S. Han, C. Yang, Y. Zhang, G. Wang, and M. Lei, "Weighted DFT codebook for multiuser MIMO in spatially correlated channels," in *Proceedings of the IEEE 73rd Vehicular Technology Conference (VTC '11)*, pp. 1–5, May 2011.